PERGAMON

International Journal of Heat and Mass Transfer 45 (2002) 1007–1015

International Journal of HEAT and MASS TRANSFER

www.elsevier.com/locate/ijhmt

Modeling and experimental observation of evaporation from oxidizing molybdenum particles entrained in a thermal plasma jet

Y.P. Wan [a,*], J.R. Fincke [b,1], S. Sampath [c], V. Prasad [c], H. Herman [c,2]

[a] *Center for Thermal Spray Research, State University of New York at Stony Brook, Stony Brook, NY 11794-2275, USA*
[b] *Idaho National Engineering and Environment Laboratory, ID 83415-2211, USA*
[c] *Center for Thermal Spray Research and Process Modeling Laboratory, State University of New York at Stony Brook, Stony Brook, NY 11794-2275, USA*

Received 22 January 2001; received in revised form 30 June 2001

Abstract

A model describing the in-flight evaporation of particles injected into a high-temperature plasma jet issuing into surrounding air has been developed and incorporated into an earlier model that includes a detailed description of particle heating and melting. In addition to physical evaporation controlled by vapor diffusion and heat transfer, the evaporation due to the production of volatile oxides on the particle surface is also modeled. The effect of evaporation-induced mass transfer on heat flux to the particle surface is taken into consideration along with the effects of variable plasma properties and the modification of heat and momentum transfer due to non-continuum effects experienced under plasma conditions. Computational results on molybdenum particles in an argon–hydrogen DC plasma spray system are developed and are qualitatively compared with experimental results.

Keywords: Evaporation; Oxidation; Plasma spray; Molybdenum; Modeling

1. Introduction

The thermal plasma spray process is a process widely used for the production of high-performance metallic and ceramic coatings. In this process micron-sized (5–100 μm) particulates are injected into a high-temperature plasma stream. The particulates are subsequently melted, accelerated and impacted on a substrate to form a coating. The process is most often performed in a normal laboratory environment with the plasma jet issuing into surrounding air.

Evaporation of powder materials during plasma spraying is a common phenomenon that has recently attracted considerable attention from researchers and engineers in the thermal spray field. The evaporation process itself may not directly cause deleterious effects to the quality of the coatings produced, but it does significantly affect the heating of particles in-flight and introduces potentially harmful vapor into the environment that can alter the thermo-physical properties of the gas mixture. Since evaporation directly influences the momentum, heat and mass transfer between the plasma gas and powder particles, an understanding of this phenomenon is essential to the effective control of the thermal plasma spray deposition process and has even greater implications in reactive plasma spraying where particle chemical reactions are promoted.

* Corresponding author. Present address: GT Equipment Technologies, Inc., 472 Amherst Str., Nashua, NH 03063, USA.

E-mail addresses: wan@gtequipment.com (Y.P. Wan), jfl@inel.gov (J.R. Fincke), ssampath@ms.cc.sunysb.edu (S. Sampath).

[1] Tel.: +1-208-526-2031; fax: +1-208-526-2814.

[2] Tel.: +1-631-632-9512; fax: +1-631-632-7878.

0017-9310/02/$ - see front matter
PII: S0017-9310(01)00214-9

Nomenclature

A	rate constant, kg/m^2 s, Eq. (7)
B	mass transfer number, Eq. (3)
$c_{p,\mathrm{f}}$	specific heat capacity of gas at the film temperature, J/kg K
d_p	particle diameter, m
D_g	diffusivity of gas, m^2/s
E	activation energy, J/mol, Eq. (7)
f_kn	factor for non-continuum effect, Eq. (9)
f_v	factor for evaporation effect, Eq. (11)
h	heat transfer coefficient, W/m^2 K
h_m	mass transfer coefficient, kg/m^2 s, Eq. (9)
k_f	thermal conductivity of gas at the film temperature, W/m K
L_v	latent heat of vaporization, J/kg, Eq. (5)
$\dot{m}_\mathrm{v}$	evaporation rate, kg/s, Eqs. (3) and (5)
$\dot{m}''_\mathrm{ox}$	oxidation rate, kg/m^2 s
Nu	Nusselt number $= hd_\mathrm{p}/k_\mathrm{f}$
Pr	Prandtl number $= \mu c_{p,\mathrm{f}}/k_\mathrm{f}$
$\dot{q}''_\mathrm{c}$	convective heat transfer to particle surface, W/m^2, Eq. (12)
$\dot{Q}_\mathrm{net}$	net heat transfer to particle surface, W, Eq. (5)
r_p	radius of particle, m
R	gas constant, J/mol K, Eq. (7)
Re_p	Reynolds number, $Re_\mathrm{p} = \bar{\rho} u_\mathrm{rel} d_\mathrm{p}/\mu$, Eq. (10)
Sc	Schmidt number, $Sc = \bar{\rho} D_\mathrm{g}/\mu$, Eq. (10)
Sh	Sherwood number, $Sh = h_\mathrm{m} d_\mathrm{p}/(\bar{\rho} D_\mathrm{g})$, Eq. (9)
$S_{\tilde{\varphi}}$	source term, Eq. (14)
T	oxidation temperature or surface temperature, K
$\tilde{T}$	Favre-averaged gas temperature, K
T_m	melting temperature, K
T_tr	transition temperature, K
$\tilde{u}$	Favre-averaged radial velocity, m/s
u_rel	relative velocity between particle and gas, m/s
$\tilde{v}$	Favre-averaged axial velocity, m/s
x	radial coordinate in cylindrical system, m
y	axial coordinate in cylindrical system, m
$\tilde{Y}_\mathrm{O}$	local mass fraction of oxidant in surrounding gas, Eq. (8)
Y^*_O	mass fraction of gas-phase oxidant at particle surface, Eq. (8)
$\tilde{Y}_\mathrm{v}$	local mass fraction of vapor in surrounding gas, Eq. (4)
Y^*_v	mass fraction of vapor at particle surface, Eq. (4)

Greek symbols

$\tilde{\varphi}$	general variable for turbulent parameters, Eq. (14)
μ	laminar dynamic viscosity of gas, kg/s m
μ_t	turbulent dynamic viscosity of gas, kg/s m
$\bar{\rho}$	density of gas, kg/m^3
$\sigma_{\tilde{\varphi}}$	Prandtl number, Eq. (14)

In most situations, the evaporation of high-temperature particles can be attributable to two different mechanisms. One is the physical evaporation where the material changes from solid (s) or liquid (l) into vapor (g) phase. This happens generally when the temperature approaches the boiling point of this material. There is no change of component in physical evaporation, which can be simply expressed as

$$\mathrm{M(s,l)} + Q = \mathrm{M(g)}, \tag{1}$$

where Q is the latent heat of evaporation of material M.

The second mechanism of evaporation occurs when volatile components are formed by chemical reactions on the particle surface. This is mostly commonly due to oxidation in the case of metallic powders. We will limit our discussion in this paper to the production of volatile oxides. The mechanism can be written as

$$\mathrm{M(s,l)} + \frac{x}{2}\mathrm{O_2(g)} = \mathrm{MO}_x\mathrm{(g)}. \tag{2}$$

Both evaporation mechanisms are possible in plasma spraying process, depending on the powder material, particle temperature and oxidant content of the ambient gas. The source of the oxygen is controlled by entrainment of the surrounding atmosphere (air).

The physical evaporation of molten droplets has been previously modeled with several papers published on the topic. Most modeling studies that include evaporation [1,2] assume that the heat flux at the particle surface is the rate-controlling mechanism for evaporation, i.e., evaporation takes place only after the particle temperature (or surface temperature) has reached the boiling point. This simplified treatment ignores the evaporation from the surface of a particle at temperatures lower than the boiling point, and the possibility of the formation of volatile species through thermal decomposition or reaction with the surrounding gas. While the consideration of mass-diffusion-controlled evaporation is rather common in the research of droplet combustion [3], knowledge on its role in thermal spray analysis is very limited. Fiszdon [4] is probably the first author who investigated the phase change of an alumina particle in a plasma jet and included the diffusion of vapor. Later, both the Langmuir evaporation and mass transfer of species across the boundary layer were included by Westhoff et al. [5] in their model through the harmonic average of two mass transfer coefficients. Vardelle et al. [6] have recommended that the Langmuir expression is only applicable to the vacuum environment while the mass diffusion must be considered for spraying

under atmospheric conditions. Although no detailed evaporation calculations under real plasma spray conditions have been reported in the above-mentioned publications, the basic transport phenomena associated with the evaporation of in-flight particles are discussed in detail in these papers.

Evaporation is complicated by chemical reactions on the particle surface. Very few studies, either experimental or theoretical, have considered this effect. Because of the complex nature of heterogeneous oxidation or other chemical reactions, this mode of evaporation is inevitably material dependent. Many different kinds of chemical reaction can cause mass loss from the particle. As discussed by Westhoff et al. [5], alumina droplets can be evaporated through decomposition into volatile AlO and O_2, the evaporation rate determined by the mass transfer of AlO vapor from the droplet surface under equilibrium reaction conditions. Oxidation of powder materials (e.g., molybdenum [7]), is another mechanism of vapor production. The formation of volatile molybdenum oxides will be taken as an example in this paper.

A major consequence of evaporation is the effect of mass transport on convective heat transfer. This is a well-studied phenomenon in droplet combustion [3,8]. In plasma spray processing, this important effect was first addressed by Chen and Pfender [9]. Their analytical results of heat and mass transfer from a single particle exposed to thermal plasma with a fixed temperature show severe reductions in heat transfer to the particle because of surface evaporation. Although the importance of this effect has also been mentioned by a few other thermal spray researchers [10], a comprehensive model that accounts for particle movement, oxidation and heating including the effect of evaporation on heat and mass transfer has not been developed, and no systematic study has been conducted to analyze these effects under transient plasma conditions.

It remains a formidable challenge to obtain quantitative data on particle evaporation, such as the change in particle size and vapor concentration in the plasma jet. Although considerable experimental data are available on particle trajectory, velocity, surface temperature and particle size, they cannot be used directly to study each of the evaporation effects as discussed in the previous paragraphs since such experimental data represent all of the physical phenomena in an integrated manner. It is evident that only a comprehensive model can provide information on each individual phenomenon as well as their combined effects. The purpose of this paper is to develop such a model for particle evaporation under plasma spray conditions. The significance of each individual effect is analyzed by performing calculations for molybdenum powders sprayed in an argon–hydrogen DC plasma system. A qualitative comparison with experimental data is also presented.

2. Mathematical model

Previously, we have developed a detailed model [11] for particle heating, melting, physical evaporation and resolidification. In this model the particle is assumed to be spherical. The one-dimensional heat conduction equation with phase change within the particle is solved numerically. Physical vaporization and its effect on convective heat transfer were included along with modifications for non-continuum behavior in the thermal plasma environment. Here, we will highlight only the details related to physical evaporation and develop the treatment used to account for the effects of the formation of volatile oxides.

2.1. Physical evaporation

The evaporation rate controlled by vapor diffusion through the boundary layer around the particle [3] can be expressed by

$$\dot{m}_{\mathrm{v}} = 2(\bar{\rho}D_{\mathrm{g}})_{\mathrm{f}}\pi r_{\mathrm{p}}\ln(1+B)Sh, \tag{3}$$

where the Sherwood number, Sh, accounts for convective mass transfer. The mass transfer number, B, is related to the local mass fraction of vapor in the gas phase, $\tilde{Y}_{\mathrm{v}}$, and the vapor concentration on the particle surface, Y_{v}^*, and is defined as

$$B = \frac{Y_{\mathrm{v}}^* - \tilde{Y}_{\mathrm{v}}}{1 - Y_{\mathrm{v}}^*}. \tag{4}$$

The vapor concentration on the particle surface, Y_{v}^*, is determined by the temperature dependence of the vapor pressure of the particulate material. The evaporation rate increases rapidly as the particle surface temperature approaches the boiling point. Ultimately the rate of evaporation is limited by the rate of heat transport to the particle surface. As soon as the product of the rate of evaporation (determined by Eq. (3)) by the latent heat of evaporation exceeds the rate of heat transfer to the particle surface, the rate of heat transfer limits the rate of evaporation. At this point the rate of evaporation is simply expressed as

$$\dot{m}_{\mathrm{v,heat}} = \dot{Q}_{\mathrm{net}}/L_{\mathrm{v}}. \tag{5}$$

2.2. Evaporation controlled by oxidation (for molybdenum particles)

The rate of formation of surface oxides can alternately be controlled by the rate of chemical reaction or the rate of transport of oxidant to the particle surface. The rate-limiting process therefore depends on the reaction kinetics determined by the surface temperature and the surrounding oxidant concentration. At a surface temperature between 500 °C and the melting point, 2622

°C, volatile oxide MoO_3 is the predominant oxide formed [12,13]. That is, a stable oxide scale is non-existent at these temperatures and a fresh metallic surface is always present. Hence, we will consider only a single reaction mechanism. The reaction is expressed as

$$\mathrm{Mo(s)} + \frac{3}{2}\mathrm{O_2(g)} = \mathrm{MoO_3(g)}. \tag{6}$$

For temperatures between 500 °C and a transition temperature T_{tr} (to be discussed below), the rate of chemical reaction on the molybdenum particle surface is the rate-determine process. Here, the transition temperature, T_{tr}, is the temperature beyond which the rate of oxidation changes from being limited by the rate of chemical reaction on the particle surface to being limited by the rate of transport of oxygen to the particle surface. That is, below T_{tr} the oxygen concentration is sufficient to supply oxidant at a rate greater than the rate at which the chemical reaction proceeds. Above the transition temperature the rate of reaction is limited by the rate of transport of oxygen to the particles' surface [12,13].

The rate of oxidation is given by Gulbransen et al. [12] as

$$\dot{m}_{ox} = A\exp(-E/RT), \quad 500\ ^\circ\mathrm{C} < T < T_{tr}. \tag{7}$$

Here, T is the surface temperature of the particle that is determined by the heat transfer between the plasma flame and particle. The coefficient A and activation energy E are given by Gulbransen et al. [12] as $10^{21.5}$ atom/cm^2 s (5.04 kg/m^2 s) and 19.7 kcal/mol (82.4 kJ/mol), respectively.

The transport of oxidizer from the gas phase to the particle surface becomes the rate-controlling phenomenon when the surface temperature exceeds the transition temperature, T_{tr}. At this point, the oxidation rate becomes equal to the diffusion rate of oxygen from the plasma gas to the surface, and is given as

$$\dot{m}_{ox} = h_m(\tilde{Y}_O - Y_O^*), \quad T_{tr} < T < 2622\ ^\circ\mathrm{C}. \tag{8}$$

Here, $\tilde{Y}_O$ is the local mass fraction of oxidant in the surrounding gas, and Y_O^* is the mass fraction of adsorbed oxygen on the particle surface, whose value is generally very small and can be set to zero. The mass transfer coefficient, h_m, can be obtained from

$$h_m = \frac{Sh(\bar{\rho}D_g)}{d_p} f_{kn}, \tag{9}$$

where the Sherwood number is calculated from [3]

$$Sh = 2.0 + 0.6Re_p^{1/2}Sc^{1/3}. \tag{10}$$

Here, Re_p is the Reynolds number based on the particle size and the relative velocity between the particle and plasma gas. In Eq. (10), the Schmidt number Sc is taken as 0.7 for the calculations presented here. The factor f_{kn} in Eq. (9) represents the influence of non-continuum effects on mass transfer. We use the same formulation for f_{kn} as the one developed to modify the heat transfer coefficient [14] to account for the Knudsen effect on mass transfer.

It is worth pointing out that the formulation of f_{kn} suggested by Chen and Pfender [14] is derived from a system without convection and evaporation. Here, we have actually made an assumption that for a system with convection and evaporation, the factor f_{kn} in Eq. (9) takes the same value as that for a system without convection and evaporation. The validation of such an assumption for a system with convection has been discussed by Chen and Pfender [15] and Chen [16].

2.3. Effect of evaporation on heat and momentum transfer

According to Faeth [3], the conventional formulation for drag coefficient still provides a good correlation in the situation of particle evaporation. The only modification needed is to include the effects of variable plasma properties [17] and Knudsen non-continuum on drag [14]. However, the Nusselt number, Nu, for convective heat transfer needs to be modified by considering the effect of evaporation in addition to the effects of variable plasma properties [17] and Knudsen non-continuum [14]. The effect of evaporation on heat transfer can be put in a single factor, f_v [3]:

$$f_v = \frac{\dot{m}_v c_{p,f}/2\pi r_p k_f}{\exp\{\dot{m}_v c_{p,f}/2\pi r_p k_f\} - 1}. \tag{11}$$

Hence, the convective heat transfer rate to the particle is given by

$$\dot{q}_c'' = h(\tilde{T} - T), \tag{12}$$

where

$$h = Nu\frac{k_f}{d_p} f_{kn} f_v. \tag{13}$$

The Nusselt number (Nu) is the function of Reynolds number (Re) and Prandtl number (Pr), and its formulation used here is based on researches in droplet combustion [3], as also used and described in our previous paper [11]. A more comprehensive study of the correlations for heat and mass transfer (Nu and Sh) in thermal plasma environment has been reported by Chen [18].

2.4. Plasma jet

In this study, the plasma jet is simulated using the two-dimensional axi-symmetric version of LAVA code [19] that solves the complete, compressible Navier–Stokes equations for a two-dimensional cylindrical coordinate system:

$$\frac{\partial(\bar{\rho}\tilde{\varphi})}{\partial t}+\frac{1}{x}\frac{\partial(\bar{\rho}x\tilde{u}\tilde{\varphi})}{\partial x}+\frac{\partial(\bar{\rho}\tilde{v}\tilde{\varphi})}{\partial y}=\frac{1}{x}\frac{\partial}{\partial x}\left(\frac{\mu+\mu_t}{\sigma_{\tilde{\varphi}}}x\frac{\partial\tilde{\varphi}}{\partial x}\right)+\frac{\partial}{\partial y}\left(\frac{\mu+\mu_t}{\sigma_{\tilde{\varphi}}}\frac{\partial\tilde{\varphi}}{\partial y}\right)+S_{\tilde{\varphi}}. \tag{14}$$

The turbulent viscosity is estimated using the standard $\tilde{k}$–$\tilde{\varepsilon}$ model. The calculation includes a representation of the chemistry of an entraining plasma jet. The reaction mechanism for the argon–hydrogen–air system considered here includes dissociation, ionization and recombination reactions, as given in our previous publication [11].

2.5. Particle movement and heating

Here, we assume that the powder particles are spherical and the particles are accelerated or decelerated mainly by drag force, which depends on the relative velocity between the particle and surrounding gas. The particles can be heated up or cooled down by the surrounding plasma gas through convection and radiation. The effects of variable plasma properties, noncontinuum and evaporation on heat transfer are all taken into consideration as previously described. Internal conduction within the particle is also considered in the present model. The particles can undergo phase change such as melting, evaporation and even resolidification based on the surrounding temperature and rate of heat transfer. The details about the particle-heating model can be found in the paper by Wan et al. [11]. Oxidation is generally an exothermic reaction and heat can be released in the reaction zone. Here, we neglect the heating of particle due to the released heat of reaction, since, as will be shown, the energy release for the amount of metal oxidized is small as compared to the magnitude of the heat transfer between plasma and the particle.

3. Results and discussion

The calculations reported here are performed for an argon–hydrogen DC plasma system with external power injection. The geometry of the spray system and validity of the computational results of the flow field for both plasma jet and injected powder particles can be found in our previous publication [11]. A series of conditions that corresponded to a range of experimental conditions were simulated. In the following sections the experimental observation and comparison to computational results will be presented. We will also examine the effects of plasma power and particle size on evaporation phenomena.

3.1. Experimental observations

A series of experiments were performed on the evaporation of plasma-sprayed molybdenum particles. As composed in Fig. 1, the laser-illuminated high-speed photographs of the torch exit region illustrate the location at which the evaporation of plasma-sprayed molybdenum particles is initiated at six different operation conditions. The six images correspond to increasing amounts of hydrogen in the plasma gas. Increased hydrogen increases the voltage of the constant current discharge. This increases the power input to the plasma, noted on the images. Molybdenum particles are injected vertically (top to bottom) through an external injector. Pictures clearly show the individual particles entering the plasma jet, their trajectory changing as they interact with the high-speed (3000 m/s) jet and the bright clouds of vapor appearing as the particles progress in the downstream direction. These bright clouds are vapor clouds surrounding evaporating particles and are apparent indicators of the location of initiation of vaporization and a qualitative indicator of the level of evaporation. The photographs were obtained with an effective shutter speed of 30 ns. The particles and vapor clouds were illuminated by a 337 nm nitrogen laser. The images were recorded by a gated, image-intensified CCD camera that was synchronized with the laser pulse.

From the pictures in Fig. 1, we conclude that: (1) larger hydrogen concentrations lead to increased evaporation of particles. (2) Visible evaporation starts at the hydrogen flow rate of 3 slm. (3) Evaporation starts earlier (closer to torch) at higher hydrogen concentrations at a downstream distance of about 1.5 cm for the 3 slm case and of about 1.0 cm for the 9 slm case. Hydrogen injection increases the power deposition in the plasma gas by increasing the discharge voltage and also enhances the heat transfer coefficient by increasing the thermal conductivity of the gas. These observations will be used for qualitative comparison with numerical results and partial validation of the present evaporation model.

3.2. Comparison of calculations with observations

Iso-contours of plasma temperature and the oxygen concentration calculated with LAVA code are plotted in Fig. 2 to illustrate the general flow field of the plasma jet. Trajectories of two particles with the size of 20 and 40 μm, respectively, are also shown in this figure.

The proposed evaporation model was used to simulate the evaporation process of plasma-sprayed molybdenum particles under the same operation conditions as in the experiments. As shown in Fig. 3, a particle with a diameter of 20 μm (10 μm radius) undergoes evaporation shortly after its injection. The evaporation terminates after the particle travels about 3 cm axially (note

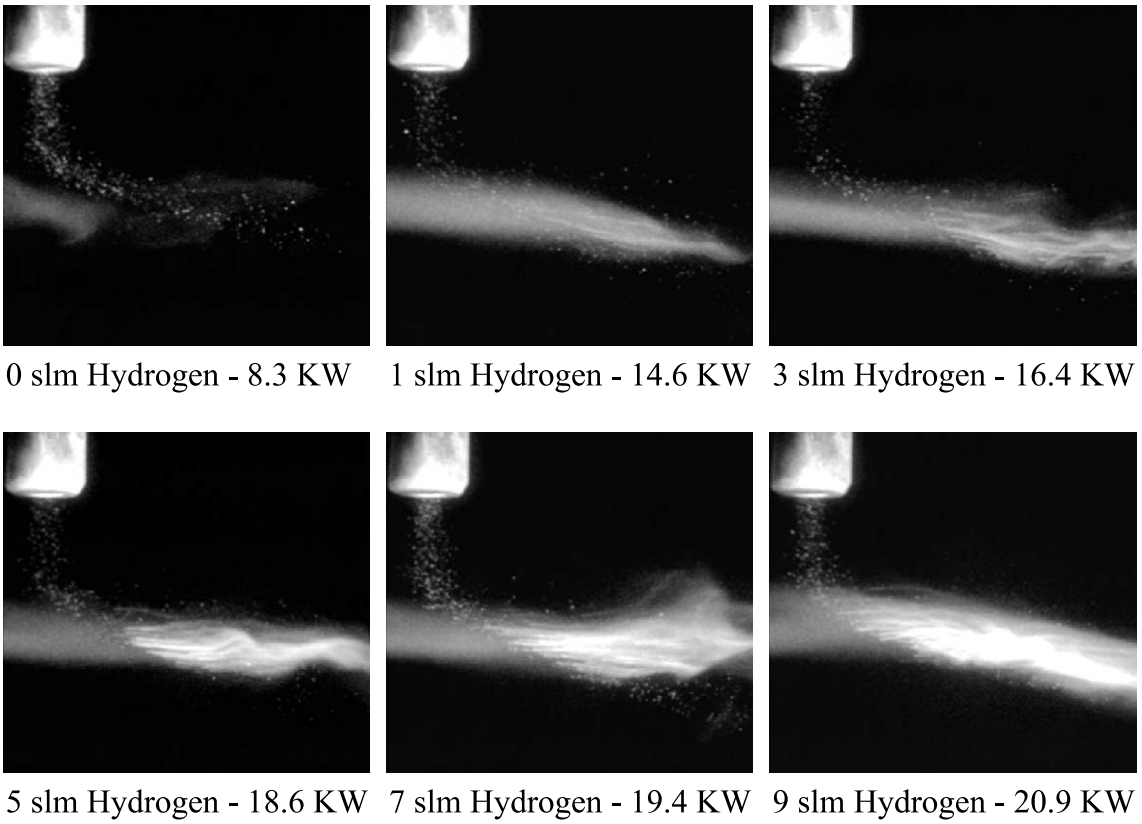

Fig. 1. Photograph of plasma-sprayed molybdenum particles near the torch exit at various hydrogen flow rates. Flow is left-to-right with the exit of the plasma torch located at the left edge of each image. Vapor clouds around the particles after traveling a short distance can be seen when hydrogen flow rate and power input to the plasma are high.

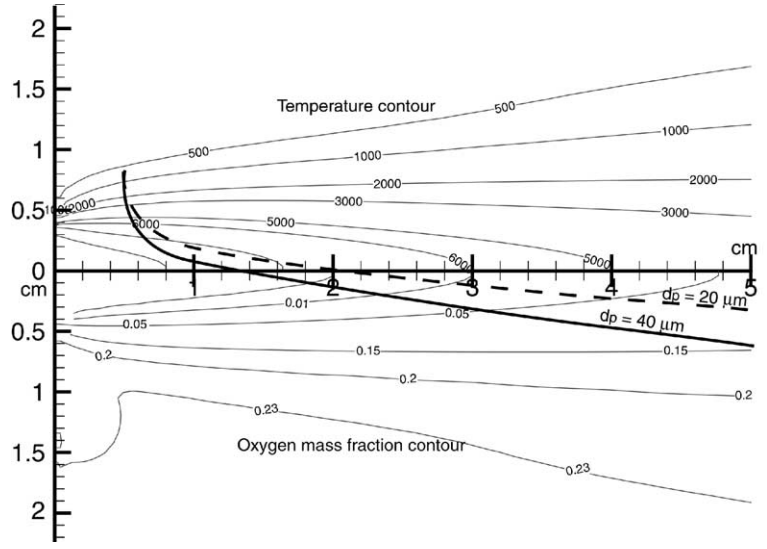

Fig. 2. Contour of gas temperature (upper part) and mass fraction of oxygen (lower part) in plasma jet, and the trajectory of two injected particles with the size of 20 (dashed line) and 40 (solid line) μm, respectively.

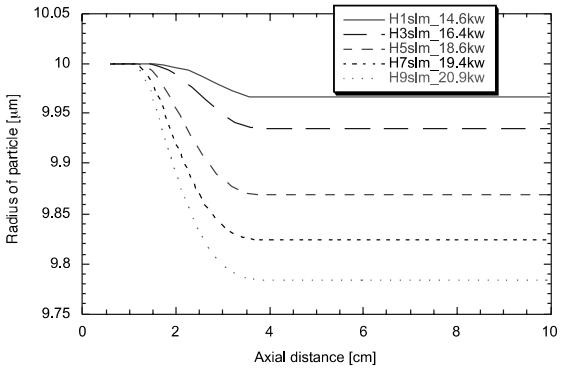

Fig. 3. Reduction of particle radius along the axial distance due to evaporation for different hydrogen flow rates.

that the injector is located at an axial coordinate of 0.6 cm). At this point the plasma temperature has decreased, as shown in Fig. 2, and the rate of heat transfer is greatly diminished. It is obvious from Fig. 3 that higher hydrogen flow rate (higher power input) results in greater evaporation (Fig. 1). The mass loss of this particle due to evaporation for the 1 slm hydrogen is less than 1%, while it is more than 6% for the highest hydrogen flow rate (9 slm). In the case of the larger hydrogen flow rates, the particle also starts evaporation earlier, as can be seen from Fig. 3. This is consistent with experimental observations shown in Fig. 1. Note that the actual particle trajectories are not identical for each case of hydrogen flow rate and plasma power input.

A higher-resolution comparison is presented in Fig. 4, where the calculated trajectories of two particles with size of 20 and 40 μm are plotted together with the starting point of evaporation. The penetration of the smaller particle into the high-speed plasma jet is less because of the greater axial acceleration. The smaller particle starts evaporation a bit earlier, after traveling about 0.7 cm axially, while the larger one starts evaporation after about 1.6 cm. The larger particles with their greater momentum penetrate further into the plasma jet. These computational results qualitatively match the visualization shown in Fig. 4, and account for the "tilt" in the location of the apparent inception of vaporization.

3.3. Effect of particle size

The evaporation rates for different sizes of particles are plotted in Fig. 5. Note that, in addition to differences in thermal mass, each particle size experiences a different trajectory, Figs. 2 and 4, and exposures to very different surrounding environments. Generally, smaller particles have larger evaporation rates, because a small particle is more readily heated up. In addition, the small particles have larger mass transfer coefficients according to Eq. (9). An exception is the behavior of the 10 μm particle, shown in Fig. 5, which exhibits a lower evaporation rate than that of a 20 μm particle. This is primarily because a 10 μm particle with an injection velocity of 9.8 m/s cannot penetrate into the hot core of the plasma jet because of its low momentum. This keeps the particle in the cooler outer region of the plasma jet resulting in less energy transfer. The present results indicate that, under the spraying conditions considered in this study, particles about 20 μm in diameter will have the highest evaporation rate.

3.4. Effect of mass transfer

The influence of mass transfer on heat transfer coefficient is demonstrated in Fig. 6. The dependency is through an evaporation parameter, f_v. This parameter is unity when there is no vaporization and is otherwise smaller than one. The very small value of this parameter at an axial distance of about 2.2 cm is due to strong vaporization resulting in a 50% reduction in heat flux from the plasma gas to the particle. Also plotted in

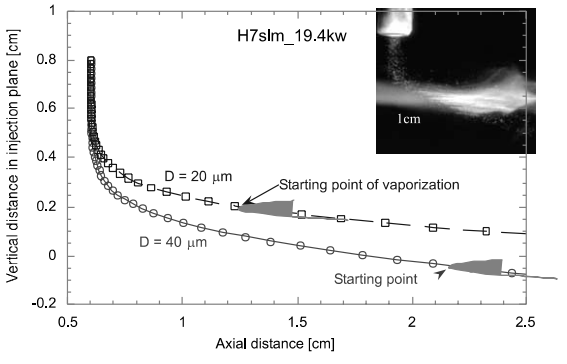

Fig. 4. Trajectories of particles with different sizes and the locations where particles start evaporating.

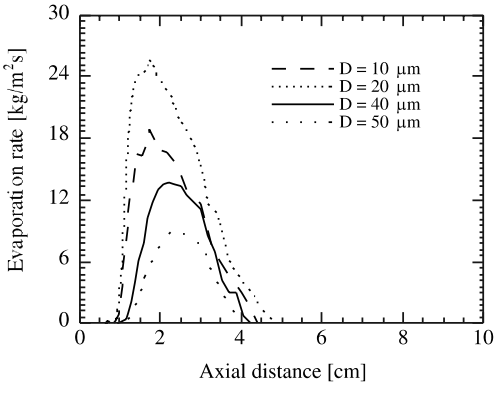

Fig. 5. Rate of evaporation for molybdenum particles of different sizes along the axial distance of plasma jet.

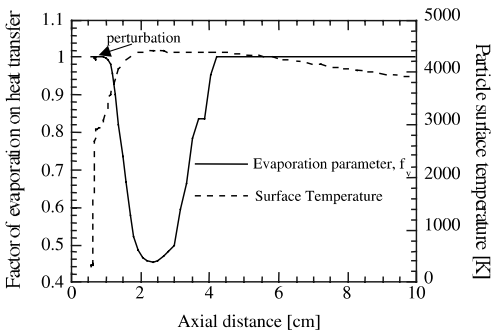

Fig. 6. Effect of mass flow due to evaporation on heat flux to the particle. Corresponding temperature of particle surface is also shown in the plot. The boiling point of molybdenum is about 4900 K.

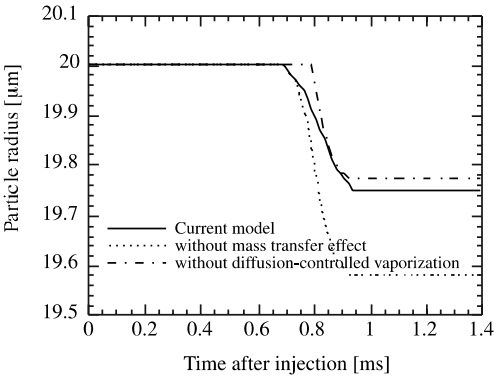

Fig. 7. Reduction of particle radius by evaporation calculated with the consideration of different effects.

Fig. 6 is the particle surface temperature. The value of f_v is less than unity even when the particle surface temperature is much lower than the boiling point (about 4900 K) due to appreciable evaporation. At temperatures less than the boiling point the evaporation is controlled by the intrinsic vapor pressure of the molybdenum and limited by diffusion of vapor through the boundary layer surrounding the particle surface. One may notice that the value of f_v returns to unity (at about 4.2 cm) even though the surface temperature is still very high. This is because the local plasma temperature is lower than the particle surface temperature and there is a net rate of heat transfer from the particle to the plasma. Thus, there is no energy available to further vaporize material.

The consequence of the evaporation model used on heat transfer is illustrated in Fig. 7. The change of particle radius has been calculated for three different cases: (1) without the influence of mass transfer on heat transfer, (2) without the effect of diffusion-controlled evaporation rate, and (3) with both effects included. From Fig. 7, it is evident that if the effect of mass transfer on heat transfer is not taken into account (case 1), the radius of the particle decreases significantly more, approximately twice as much as when this effect is included (case 3). This implies an 800% difference in the prediction of mass vaporized. On the other hand, if the diffusion-controlled vaporization is not included, i.e., assuming that the evaporation rate is controlled only by heat transfer rate (case 2), the evaporation starts a little later when the particle temperature reaches the boiling point. However, the difference in vaporization rate as presented in terms of radius reduction with and without (case 2 and case 3) diffusion-controlled vaporization is not significant. This suggests that the heat-transfer-controlled evaporation model with the mass transfer correction can be used without any appreciable error in the prediction of particle size and conditions along its trajectory while saving significantly on computation time. These results together, Figs. 6 and 7, emphasize that the effect of evaporation on heat transfer must be taken into consideration in the calculation of particle heating if evaporation is anticipated.

3.5. Effect of oxidation

In Fig. 6, a small perturbation can be noticed in the evaporation parameter, f_v, at about 0.6 cm along the axis. This is primarily due to the loss of a small amount of mass through the production of the volatile molybdenum oxide. The evaporation rate that results from it is so small that a logarithm coordinate needs to be used to show the change in evaporation rates due to oxidation and physical evaporation, as shown in Fig. 8. The first peak of evaporation rate caused by oxidation is two orders of magnitude smaller than the second one, which is produced by physical evaporation. Such a small change in evaporation rate (0.1 kg/m^2 s) does not significantly alter the particle diameter, Fig. 3. Therefore, for molybdenum particles under the plasma spray con-

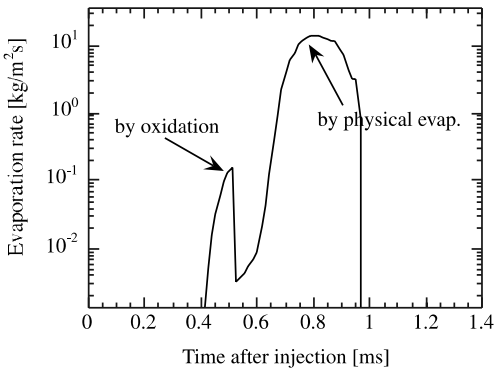

Fig. 8. Evaporation rate caused by oxidation and physical vaporization during the flight of a 40 μm molybdenum particle.

ditions considered here, the amount of mass loss caused by production of a volatile oxide can be neglected.

4. Conclusions

A model for vaporization of plasma-sprayed molybdenum particles that includes formation of a volatile surface oxide and physical evaporation is developed. The effect of mass diffusion due to evaporation on surface heat flux is also included in the model. The computational model predicts the location of the onset of vaporization and the effect of particle size distribution. The results are in qualitative agreement with experimental observations. The importance of evaporation in thermal spray processing is its influence on the rate of heat transfer. The use of a simplified evaporation model that considers heat transfer as the rate-controlling phenomenon is justified by the small difference between the predicted size change of particles using models with and without consideration of mass-diffusion-controlled evaporation. For molybdenum particles, the production of volatile oxide on the surface contributes little to the total loss of particle mass due to vaporization, in fact the evaporation due to oxidation is two orders magnitude smaller than that due to physical evaporation. The smaller particles generally have higher evaporation rates than the larger particles, as long as the injection velocity is high enough for the particle to penetrate into the core of the plasma jet.

Acknowledgements

This research was supported by the National Science Foundation through the MRSEC Program under Award No. DMR-9632570, and the US Department of Energy under the DOE Idaho Field Office contract DE-AC07-94ID13223. Department of Energy funding was provided by the DOE-ER, Office of Basic Energy Sciences, Engineering Research Program.

References

[1] P. Proulx, J. Mostaghimi, M.I. Boulos, Plasma–particle interaction effects in induction plasma modeling under dense loading conditions, Int. J. Heat Mass Transfer 28 (1985) 1327–1336.

[2] D.K. Das, R. Sivakumar, Modeling of the temperature and the velocity of ceramic powder particles in a plasma flame – I. Alumina, Acta Metall. Mater. 38 (1990) 2187–2192.

[3] G.M. Faeth, Evaporation and combustion of sprays, Prog. Energy Combust. Sci. 9 (1983) 1–76.

[4] J.K. Fiszdon, Melting of powder grains in a plasma flame, Int. J. Heat Mass Transfer 22 (1979) 749–761.

[5] R. Westhoff, G. Trapaga, J. Szekely, Plasma–particle interactions in plasma spraying systems, Metall. Trans. B 23 (1992) 683–693.

[6] A. Vardelle, N.J. Themelis, B. Dussoubs, M. Vardelle, P. Fauchais, Transport and chemical rate phenomena in plasma sprays, J. High Temp. Process. 1 (1997) 295–314.

[7] Y.P. Wan, J.R. Fincke, S. Sampath, V. Prasad, Modeling the in-flight oxidation of plasma sprayed molybdenum particles, in: M. Hrabovsky, M. Konrad, V. Kopecky (Eds.), Proceedings of 14th International Symposium on Plasma Chemistry, International Union for Pure and Applied Chemistry, The Institute of Plasma Physics, Prague, Czech Republic, 1999, pp. 1983–1988.

[8] C.K. Law, Recent advances in droplet vaporization and combustion, Prog. Energy Combust. Sci. 8 (1982) 171–201.

[9] X. Chen, E. Pfender, Heat transfer to a single particle exposed to a thermal plasma, Plasma Chem. Plasma Process. 2 (1982) 185–212.

[10] M. Vardelle, C. Trassy, A. Vardelle, P. Fauchais, Experimental investigation of powder vaporization in thermal plasma jets, Plasma Chem. Plasma Process. 11 (1991) 185–201.

[11] Y.P. Wan, V. Prasad, G.-X. Wang, S. Sampath, J.R. Fincke, Model and powder particle heating, melting, resolidification, and evaporation on plasma spraying processes, J. Heat Transfer 121 (1999) 691–699.

[12] E.A. Gulbransen, K.F. Andrew, F.A. Brassart, Oxidation of molybdenum 550° to 1700 °C, J. Electrochem. Soc. 110 (1963) 952–959.

[13] E.A. Gulbransen, W.S. Wysong, Thin oxide films on molybdenum, Trans. AIME Met. Div. 175 (1948) 628–647.

[14] X. Chen, E. Pfender, Effect of the Knudsen number on heat transfer to a particle immersed into a thermal plasma, Plasma Chem. Plasma Process. 3 (1983) 97–112.

[15] X. Chen, E. Pfender, Behavior of small particles in a thermal plasma flow, Plasma Chem. Plasma Process. 3 (3) (1983) 351–366.

[16] X. Chen, Heat and momentum transfer between a thermal plasma and suspended particles for different Knudsen numbers, Thin Solid Films 345 (1) (1999) 140–145.

[17] Y.C. Lee, K.C. Hsu, E. Pfender, Modeling of particles injected into a d.c. plasma jet, in: Proceedings of the 5th International Symposium on Plasma Chemistry, vol. 2, 1981, p. 795.

[18] X. Chen, Particle heating in a thermal plasma, Pure Appl. Chem. 60 (5) (1988) 651–662.

[19] J.D. Ramshaw, C.H. Chang, Computational fluid dynamics modeling of multi-component thermal plasmas, Plasma Chem. Plasma Process. 12 (1993) 299–325.